https://doi.org/10.5194/wes-2020-35
Preprint. Discussion started: 11 February 2020

eawe european academy of wind energy
Open Access WIND ENERGY SCIENCE DISCUSSIONS

Determination of the Angle of Attack on a Research Wind Turbine Rotor Blade Using Surface Pressure Measurements

Rodrigo Soto-Valle[1], Sirko Bartholomay[1], Joerg Alber[1], Marinos Manolesos[2], Christian Navid Nayeri[1], and Christian Oliver Paschereit[1]

[1]Technische Universität Berlin, Hermann-Föttinger Institut, Müller-Breslau-Straße 8,10623 Berlin, Germany
[2]College of Engineering, Swansea University, Bay Campus, Fabian Way, Swansea, SA1 8EN, UK

Correspondence: Rodrigo Soto-Valle (rodrigo.soto@campus.tu-berlin.de)

Abstract. In this paper, a method to determine the angle of attack on a wind turbine rotor blade using a chordwise pressure distribution measurement was applied. The approach uses a reduced number of pressure taps data located close to the blade leading edge. The results were compared with three 3-hole probes located at different radial positions and analytical calculations. The experimental approaches are based on the 2-D flow assumption; the pressure tap method is an application of the thin airfoil theory and the 3-hole probe method uses external probe measurements and applies geometrical and induction corrections.

The experiments were conducted in the wind tunnel at the Hermann Föttinger Institut of the Technische Unversität Berlin. The research turbine is a three-bladed upwind horizontal axis wind turbine model with a rotor diameter of $3\ m$. The measurements were carried out at rated condition with a tip speed ratio of 4.35 and different yaw and pitch angles were tested in order to compare both methods over a wide range of conditions.

Results show that the pressure taps method is suitable with a similar angle of attack results as the 3-hole probes for the aligned case. When a yaw misalignment was introduced the method captures the same trend and feature of the analytical estimations. Nevertheless, it is not able to capture the tower influence. Regarding the influence of pitching the blades, a linear relationship between the angle of attack and pitch angle was found.

1 Introduction

Determining the local angle of attack (AoA) on wind turbine blades remains one of the greatest aerodynamic challenges. At the same time, the determination of AoA is necessary in order to calculate the forces over the blade, develop accurate aeroelastic models or establish a control tool. For a 2-D airfoil, the AoA is defined geometrically as the angle between the inflow velocity and the chord line. However, on a rotating system, e.g. a blade, 3-D effects from the tip and root vortices, yaw misalignment, induction effects, among others effects, render difficult the precise determination of the AoA (Shen et al., 2009).

One option is to estimate the AoA numerically, for example from BEM codes or geometrical calculations. Sicot et al. (2008) presented a study of the turbulence effects over a wind turbine model, using the pressure distribution as an indicator of separation. The determination of the AoA was computed using a lifting line method. Maeda et al. (2008) presented experimental

https://doi.org/10.5194/wes-2020-35
Preprint. Discussion started: 11 February 2020

eawe european academy of wind energy
Open Access WIND ENERGY SCIENCE DISCUSSIONS

results of the performance of a blade section under yawed conditions, based on surface pressure measurements. The AoA was calculated according to its geometrical definition using the velocity triangle defined by the wind velocity and the rotational speed. Unfortunately, these cases rely on well known freestream conditions or do not take into account induction effects. Therefore, if a more reliable estimation is required under these conditions, it is necessary to use on-blade measurement tools.

Most of the on-blade measurements use external probes to measure the local pressure. The AoA is then obtained from the measurements based on the calibration of the external probe. Various methods have been used in the published literature to determine the AoA in experimental studies of field or model wind turbines.

Maeda and Kawabuchi (2005) performed field measurements and used two 5-hole probes to determine the local dynamic pressure and the AoA on a $10\ \mathrm{m}$ diameter wind turbine under yawed conditions. The values were phase averaged in the azimuth angle with steps of $12°$, and different yaw misalignment cases were examined, from $-45°$ to $45°$ in steps of $15°$. The results showed asymmetry along the azimuth angle, attributed to the influence of the atmospheric boundary layer. The asymmetry was also present under yawed conditions, with changes up to $10°$ for negative yaw misalignment and $2.5°$ on the positive case (see reference yaw angle in Fig. 1, left).

Petersen et al. (2015) used an arrangement of 5-hole probes at five radial positions to determine the undisturbed inflow field of a wind turbine. The method compared very well against numerical results obtained, using the code HAWC2aero (nonlinear aeroelastic implementation from the simulation code HAWC2 Larsen and Hansen (2007)). The agreement was achieved despite several issues regarding calibration, damaged sensors, and outliers present.

Gallant and Johnson (2016) presented the determination of the AoA using a 5-hole probe on a two bladed turbine model. A combination of geometrical and induction corrections, based on the work of Hand et al. (2001), was applied to obtain the AoA for different yaw offsets and tip speed ratios. The results show a good trend agreement between the probe measurements and the model proposed by Morote (2016).

In general, according to the published literature, external probes can be used to determine the AoA with sufficient accuracy. However, such probes are intrusive and significantly disturb the flow over the blade section, especially in the case of wind turbine models where probes and their mountings have dimensions comparable to the blade chord.

Other complementary tools, used on research turbines, are surface pressure sensors, located along the blade chord. These sensors are used to record the pressure distribution along the blade chord at a desired radial position and to calculate the aerodynamic loads.

It is possible to combine surface pressure sensors with probes, unfortunately, they differ in the span position, i.e. the AoA remains unknown in the specific pressure measurement position. This means that the integration of pressure can only be extended to normal and tangential forces over the blade since without knowledge of the AoA the lift and drag components cannot be calculated. This issue highlights the need for a nonintrusive method to determine the AoA over a blade section.

The National Renewable Energy Laboratory suggested an algorithm to estimate the AoA from pressure distribution values under axial (Sant et al., 2009), yaw (Sant et al., 2006a) and unsteady conditions (Sant et al., 2006b). The method assumes an initial AoA distribution. The lift is then calculated for each azimuth and radial position based on the pressure surface data and the AoA. Afterwards, the bound circulations were determined by means of the Kutta–Joukowksi theorem for a lifting line. The

https://doi.org/10.5194/wes-2020-35
Preprint. Discussion started: 11 February 2020

eawe european academy of wind energy
Open Access WIND ENERGY SCIENCE DISCUSSIONS

resulting values were prescribed in a free wake vortex model to obtain a new AoA based on the induced velocities to finally iterate until the AoA converged.

Guntur and Sørensen (2012) presented different methods to determine the AoA for the MEXICO rotor (Bechmann et al., 2011) based on CFD data. One of the approaches is based on matching up C_P distributions from 2-D and 3-D data, where the AoA was known in the former case. This method has a good agreement for small angles of attack ($< 10°$) and in the middle blade region ($0.25 \leq r/R \leq 0.85$). The latter points out an alternative method to estimate the AoA where the 2-D and 3-D pressure distribution are comparable.

Several investigations showed a relation between 2-D and 3-D pressure distribution. Ronsten (1992) showed a good agreement between the pressure distribution over nonrotating and rotating blades along span positions of $r/R \geq 0.55$ and $r/R \geq 0.3$ at tip speed ratio of 4.32 and 7.37, respectively.

Maeda et al. (2005) combined 5-hole probes and surface pressure measurements. A comparison was made between field measurements and wind tunnel experiments. The latter was carried out using the same blade in stationary conditions. The AoA was estimated through the 5-holes probes, which differs in span position from the pressure measurement section in 6% and 14%. A good agreement was shown, regarding the surface pressure distribution under prestall (AoA$= 10°$) and stall (AoA$= 16°$) conditions. In the case of a poststall (AoA$= 20°$) condition, the results of the wind tunnel present a reduced pressure magnitude on the suction side, in contrast with the field case.

Bak et al. (2011) studied the pressure distribution on a wind turbine in atmospheric conditions and in a wind tunnel. The wind tunnel experiments were carried out with 2-D wing, taking the characteristics of four specific sections from the turbine. The agreement remains valid for small angles of attack ($< 12°$) and for the outer region of the blade ($r/R > 0.4$).

Overall, it is generally agreed that static 2-D wings and rotating blades have a good agreement in surface pressure measurements, at least for attached flow conditions. This opens the possibility of using methods based on the blade chord pressure distribution to estimate the AoA, in the range of agreement.

Gaunaa (2006) developed an analytical solution for the unsteady 2-D pressure distribution on a variable geometry airfoil undergoing arbitrary motion, based on thin airfoil theory. Further investigations made by Gaunaa and Andersen (2009), using this method, related the pressure over the airfoil with the effective AoA. The added benefit of the specific method is its simplicity, as it only requires the pressure difference between the airfoil pressure and suction side at one or two chordwise positions.

This method has not been applied on a rotating blade yet. Given the good agreement between 2-D and 3-D pressure distributions away the root region, this paper presents an alternative method of determining the AoA by means of pressure taps, based on the method proposed by Gaunaa and Andersen (2009).

Nowadays, new technologies as passive fiber optic pressure sensors presented by Schmid (2017) able to perform quasistatic and unsteady measurements of rotor blades in operation that can withstand harsh conditions. Therefore, the development of new methods to determine the AoA based on pressure distribution data would provide valuable information without the necessity of invasive tools.

https://doi.org/10.5194/wes-2020-35
Preprint. Discussion started: 11 February 2020

The Technical University of Berlin has developed a scaled wind turbine model, the Berlin Research Turbine (BeRT), equipped with 3-hole probes and pressure taps on one of its blades (Vey et al., 2015). The present focuses on determining the AoA over the BeRT blades and complements previous investigations on BeRT, such as inflow modifications (Bartholomay et al., 2017), bending moment crosstalk effects (Bartholomay et al., 2018a), load alleviation with flaps (Bartholomay et al., 2018b), wind tunnel modeling (Klein et al., 2018) and wind turbine wakes (Marten et al., 2018, 2019). The results presented here are the first on-blade pressure measurements from the BeRT blade and can be used to validate numerical solvers and to develop control strategies.

In the remaining of the paper, the facilities and the research turbine model are described, followed by the methodology to determine the AoA and to assess the validity of the Gaunaa method on the rotating plane. The results are presented in Sect. 4 and the paper closes with concluding remarks in Sect. 5.

2 Experimental setup

2.1 Wind tunnel

The tests were conducted at the Hermann Föttinger Institut of the Technische Universität Berlin in the GroWiKa (large wind tunnel), a closed-loop wind tunnel driven by a $450kW$ fan, presented in Fig. 1 (left). The turbine model was placed at the large test section, where the maximum velocity is $10\ \mathrm{ms}^{-1}$.

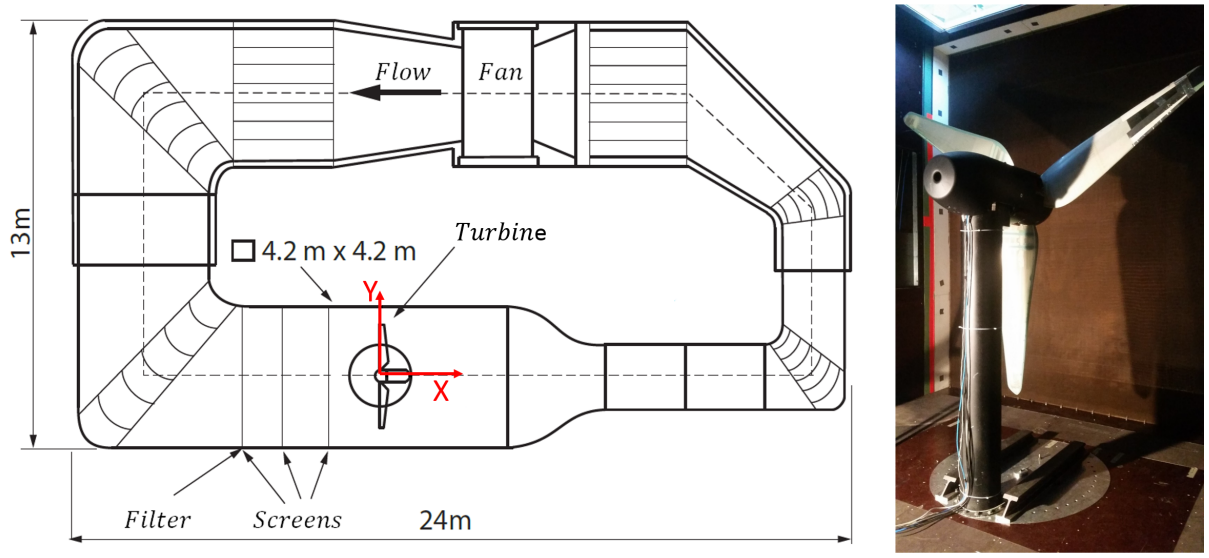

Figure 1. Outline of GroWiKa (left), Berlin Research Turbine - BeRT in the wind box (right).

https://doi.org/10.5194/wes-2020-35
Preprint. Discussion started: 11 February 2020

eawe european academy of wind energy
Open Access WIND ENERGY SCIENCE DISCUSSIONS

The setup was reproduced from the work of Bartholomay et al. (2017), in which the flow quality was measured and the reproducibility of the flow was evaluated. In order to keep the turbulence intensity on a comparable level, one homogeneous filtermat and three screens were positioned in the crosssections upstream of the turbine as it can be seen in Fig. 1 (left). The turbulence intensity achieved with this setup is less than 1.5%.

The dynamic pressure is monitored by two Prandtl tubes located at the walls at 0.86R upstream the turbine at $2.7\ m$ height. For this study, all test cases were conducted with a free stream velocity of $U_\infty \approx 6.5\ \mathrm{ms}^{-1}$.

2.2 Wind turbine model

BeRT, Fig. 1 (right), is a three-bladed upwind horizontal wind turbine with a rotor radius of $R = 1.5\ m$. The turbine yaw angle and the blade pitch angle can be modified depending on the test requirements. Figure 2 (left) shows a reference sketch for the azimuth (ϕ) and yaw (ψ) angles.

The Clark Y airfoil profile is used along the entire blade span and there is no cylindrical root section. The specific airfoil profile was chosen as it performs well at low Reynolds number (Re), i.e. at the conditions relevant to BeRT (Re range from 1.7×10^5 to 3.0×10^5 along the span). The blade twist was selected so that the local AoA stays constant over the span at rated conditions. Figure 2 (right) illustrates the definition of the main angles over a blade section and Fig. 3 (left) shows the twist and chord distributions.

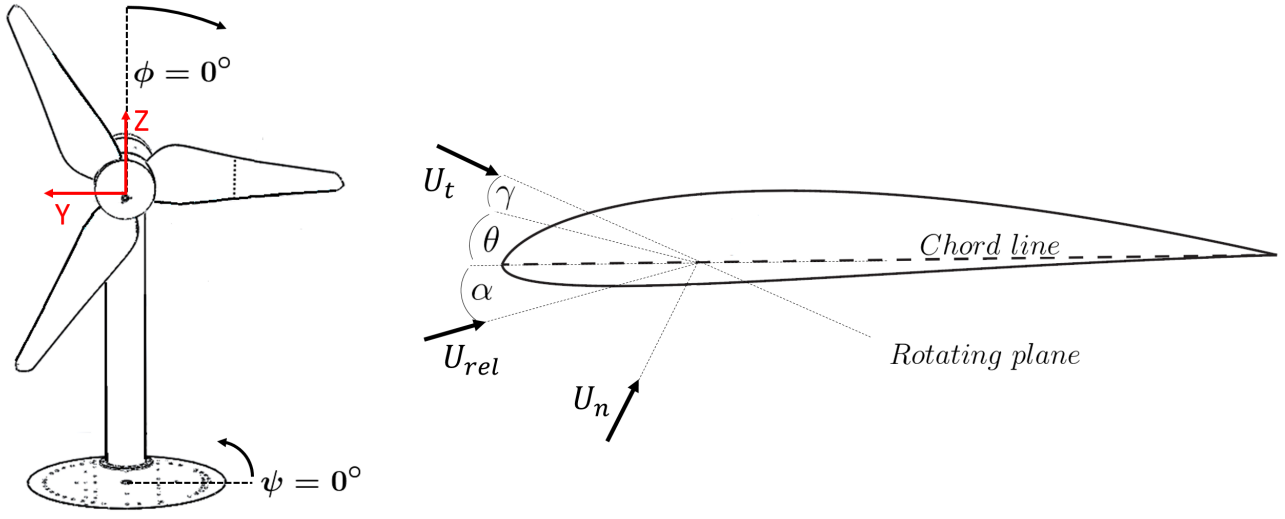

Figure 2. Angles definition. left side: Azimuth, ϕ and yaw, ψ. Right side: angle of attack, α, pitch, θ and twist, γ.

https://doi.org/10.5194/wes-2020-35
Preprint. Discussion started: 11 February 2020

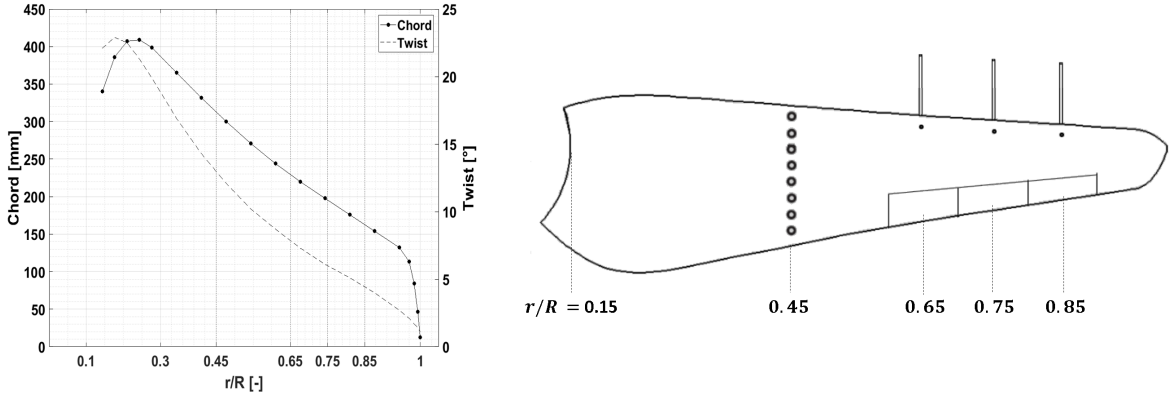

Figure 3. Twist and chord distribution along span (left). The rotor blade with 3-hole probes and pressure taps over span position (right).

One of the blades was equipped with pressure taps and three 3-hole probes at different radial positions, as shown in Fig. 3 (right). The pressure taps were located at $r/R = 0.45$. Each pressure tap was connected through silicone tubes inside the blade to a pressure box located in the hub which contains all sensors. The average length for the tubes between tap and sensor was $650mm$ which included an arrangement between cannulas and tubes as shown in Fig. 4.

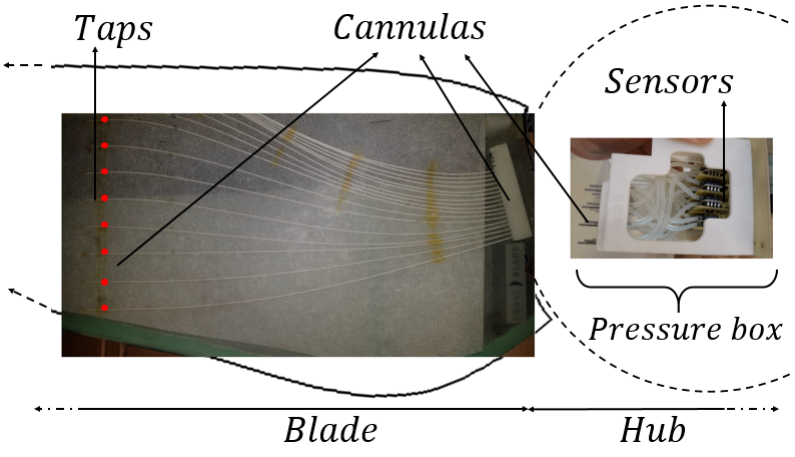

Figure 4. Tubing details between pressure taps and sensors.

The 3-hole probes were located at 65, 75 and $85\%R$ and mounted on the pressure side (see Fig. 5, left). The 3-hole probes consist of one straight tube in the middle, accompanied by two outer tubes with a $45°$ nozzle (see Fig. 5, right). Each outer tube was connected to a differential pressure sensor through a silicone tube, using the middle one as a reference. The sensors were installed at the spanwise position of each probe, reducing the tube length to less than 100 mm.

https://doi.org/10.5194/wes-2020-35
Preprint. Discussion started: 11 February 2020

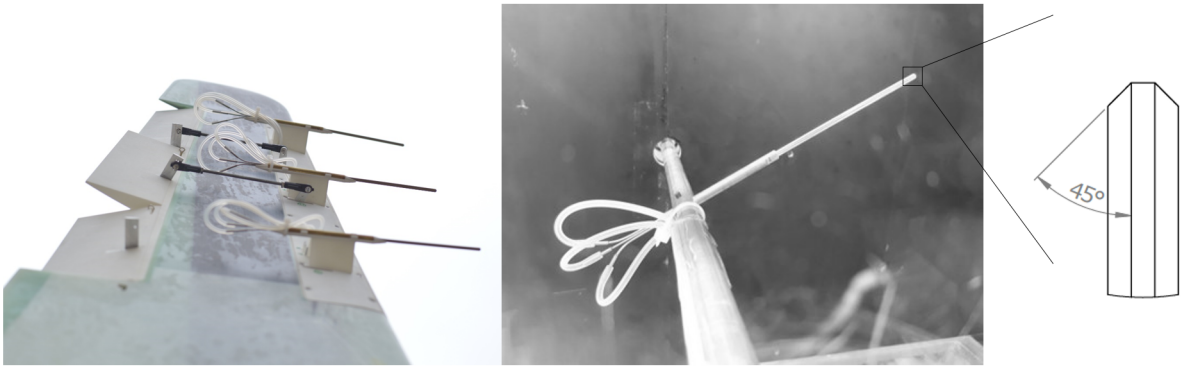

Figure 5. 3-hole probes mounted in the equipped blade (left). Calibration of a 3-hole probe and tip details (right).

All pressure transducers were installed in such a way that their membranes were parallel to the plane of rotation to minimize the centrifugal effect on them. More information about the sensors can be found in previous work by Vey et al. (2015), while the calibration and data acquisition procedure is detailed in the Sect. 3.1.

The blade was also provided with three trailing edge flaps with $10\%R$ span length and $30\%c$ chord length and located consecutively from 60% to 90% along the span. The flaps were fixed without any deflection for all test cases presented in this study. The turbulence transition was not fixed over the blades, in contrast to the previous work of Klein et al. (2018).

Rotating (NI cRIO 9068) and nonrotating (NI cDAQ 9188) measurement systems were synchronized and located in the hub and the external control cabinet, respectively. The measurement data were recorded using NI 9220 modules with an acquisition frequency of $10\ kHz$.

The pressure data from the blade were recorded through the rotating system, while the freestream dynamic pressure through the nonrotating system. The blade position was recorded through a Hall effect sensor located in the nacelle. Each measurement was recorded and phase averaged until 100 rotations were completed, with an azimuth step of $\Delta\phi = 1°$.

3 Methodology

In this section, the methodology of this research is described. The main idea is to compare the results obtained by the method proposed by Gaunaa and Andersen (2009) when is applied to the pressure tap data against the AoA from the 3-hole probe measurements and analytical calculations.

According to the BeRT design specification, the combination of chord and twist distribution achieves an optimal shape (Pechlivanoglou et al., 2015) which provides a constant AoA over most of the blade span Bartholomay et al. (2017), so the AoA at the radial position of the pressure taps and the 3-hole probes should be the same under aligned flow conditions.

The calibration of the sensors, the applied corrections and the description of the methods used to determine the AoA follow, while the test cases and their uncertainty are summarized at the end of this section.

https://doi.org/10.5194/wes-2020-35
Preprint. Discussion started: 11 February 2020

eawe european academy of wind energy
Open Access WIND ENERGY SCIENCE DISCUSSIONS

3.1 Calibration

Differential pressure sensors were used for both experimental methods, the pressure taps ($HCL0025E$) and the 3-hole probes ($HCL0075E$). During the calibration of the sensors, the turbine was in a static position and a constant pressure was provided to achieve eleven calibration pressure points using the external calibrator, Halstrup KAL 84. All calibrations were linear and the fitting curves showed a coefficient of determination values of $R^2 \geq 0.999$.

The 3-hole probes were calibrated in a small wind tunnel. The calibration range was from $-30°$ to $30°$ with steps of $0.5°$. The calibration was made between the normalized pressure and the swept angles following the standard procedure described by Dudzinski and Krause (1969). Subsequently, the calibration was repeated for inflow velocities from 16 to 22 ms^{-1} with steps of $\Delta U = 2\ \mathrm{ms}^{-1}$. The velocity range was selected so that it covers the relative velocity perceived by the blade in the range $0.45 \leq r/R \leq 0.85$, i.e. the location of the 3-hole probes. The AoA fit remains linear within -10 to $10°$, getting a nonlinear fit for larger angles.

3.2 Pressure correction

The pressure tap sensors measure differential pressure (P_{si}); one side was connected to each tap (P_i) and the other to the static pressure in test the section (P_{ref}), Eq. 1. The centrifugal effect, $P_{ctf} = 0.5\rho(\Omega r_i)^2$, Eq. 2, was quantified and corrected, based on Hand et al. (2001), where r_i is the radial position of the pressure tap i and Ω is the turbine angular velocity, $2\pi f$.

$$P_{si} = P_i - P_{ref}, \tag{1}$$

$$P_{corr} = P_{si} + P_{ctf}. \tag{2}$$

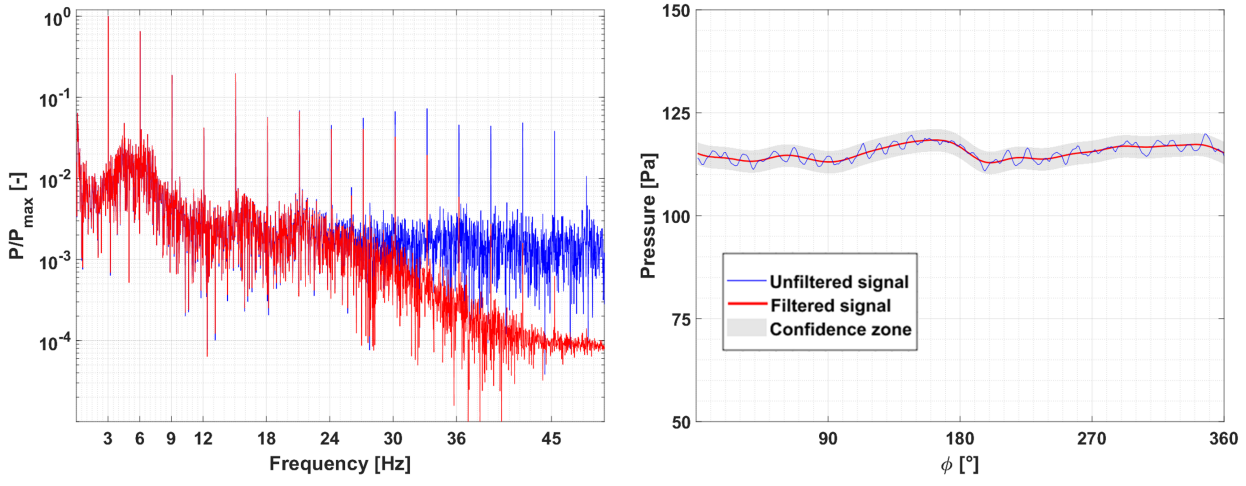

Figure 6. Comparison between filter and unfiltered signals of pressure tap at $x = 2\%c$. Frequency spectrum (left). Corrected pressure (right).

https://doi.org/10.5194/wes-2020-35
Preprint. Discussion started: 11 February 2020

eawe european academy of wind energy
Open Access WIND ENERGY SCIENCE DISCUSSIONS

Moreover, the data were filtered for high frequencies using a Butterworth filter with a cut off frequency of 30 Hz to reduce noise and the vibrations from the probe and blade. Figure 6 (left) shows the signal spectrum of the pressure tap at $x = 2\%c$. As can be seen, the main variations are influenced by the rotational frequency of 3 Hz and its harmonics. Furthermore, Fig. 6 (right) shows the corrected pressure, P_{corr} and its filtered signal of the pressure tap at $x = 2\%c$. Additionally, a confidence zone was plotted in order to quantify the uncertainty due to the filter and is addressed in Sect. 3.4.

The impact on the dynamic response through the tubes was evaluated theoretically following the model formulation of the dynamic behavior on tubes proposed by Bergh and Tijdeman (1965) and showing no significant influence in the main frequency peaks of the sensors ($1p$ and $2p$). This agrees with the previous work of Sicot et al. (2008) that used a similar setup and tube length.

The hydrostatic correction has less impact since all the sensors are located in the hub, and was consequently neglected.

3.3 Methods to determine the angle of attack

3.3.1 3-hole probes

The method to determine the AoA from the 3-hole probes was based on previous work with the same setup. It is outlined here for completeness, while further details can be found in Bartholomay et al. (2017). Figure 7 shows the reference system for an arbitrary blade section, with 3-hole probe installed.

The AoA relative to the probe, α_{probe}, was identified from the 3-hole probe calibration. However, as shown in Fig. 7, a geometrical rotation between the probe and the section coordinates was necessary to evaluate the AoA in the respective blade section, $\alpha_{probe,section}$. The latter angle differs from α, which is the effective AoA of the blade section, because of the blade itself induces a velocity on its surroundings. To correct this, XFOIL (Drela and Youngren, 2001) calculations were used to estimate the velocity at the probe location, under the assumption of 2-D flow. Afterwards, a fit function was found between the effective AoA, α, and $\alpha_{probe,section}$.

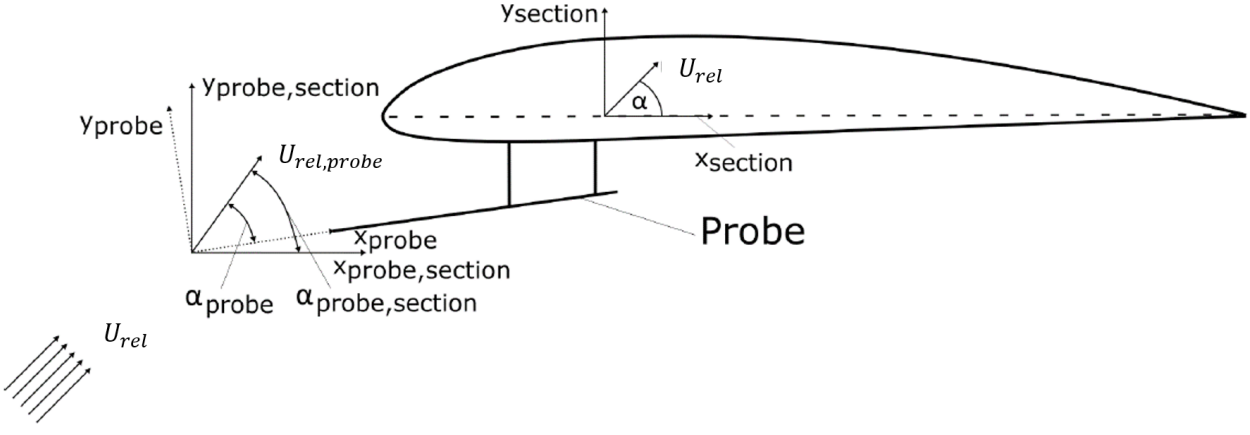

Figure 7. Schematic of the reference system for a probe, modified from Klein et al. (2018).

https://doi.org/10.5194/wes-2020-35
Preprint. Discussion started: 11 February 2020

eawe european academy of wind energy
Open Access WIND ENERGY SCIENCE DISCUSSIONS

3.3.2 Pressure taps

The determination of the AoA from the pressure distribution on the blade section was based on the unsteady model developed by Gaunaa (2006). The main assumptions for this methodology rely on the thin airfoil theory and low Mach number. This allows modeling the airfoil as its camberline together with the assumptions of inviscid, incompressible, and irrotational flow.

Aiming at simpler solutions to estimate airfoil loads that can be applied on active load control, and based on the considerations mentioned above Gaunaa (2006) formulated an analytical expression for the forces over an arbitrary airfoil shape. This expression relates the pressure difference between the lower and upper side, over the camberline, with the velocity potential field, aerodynamic forces, and pitching moment. Gaunaa and Andersen (2009) summarized this formulation in Eq. 3, as the normalized pressure and its contributions, where $\Delta P(\mathbf{x})$ is the pressure difference between the lower and upper side at a specific chordwise position and $q = 0.5\rho U^2$ is the dynamic pressure.

$$\frac{\Delta P(\mathbf{x})}{q} = g_c(\mathbf{x})\alpha_{c,eff} + g_{camb}(\mathbf{x}) + g_{\dot{\alpha}}(x)\frac{\dot{\alpha}c}{U} + g_\beta(\mathbf{x})\beta + g_L(\ddot{y}, \ddot{\alpha}, \dot{\beta}, \ddot{\beta}, \mathbf{x}). \tag{3}$$

It is important to note that this summary neglects the chord streamwise degree of freedom, i.e. $\dot{X} = \ddot{X} = 0$.

On the right side of Eq. 3, $g_c(\mathbf{x})$ corresponds to the influence of the circulatory forces. This contribution is modulated by $\alpha_{c,eff}$, the effective AoA that takes into account the time lag effects caused by the vorticity shed into the wake, for simplicity, now considered as α.

The remaining contributions in Eq. 3 depend on the instantaneous motion of the airfoil, known as added mass terms. The second and third terms, g_{camb} and $g_{\dot{\alpha}}$ correspond to the added mass due to the basic camber line and pitching, respectively.

The formulation allows the calculation of the effect of a flap on the airfoil, with β being the flap angle. This contribution in the model is considered with the added mass term g_β. Since there is no flap at the 45% span position, the flap deflection angle is set to $\beta = 0°$ and therefore g_β is eliminated.

The term g_L contains the nonlinear contributions. Gaunaa and Andersen (2009) described that the addition of the geometrical nonlinearities does not change the conclusions from linear estimation for the most part of the chord, except for a zone very close to the leading edge. Based on this consideration, the term g_L is neglected.

Gaunaa and Andersen (2009) and Velte et al. (2012) suggested a control variable based only on two pressure taps. To achieve this, the contribution of the pitching added mass term, $g_{\dot{\alpha}}$ was neglected by choosing a specific chord position where its value is zero.

Equation 4 shows the reduced relation between pressure distribution and AoA, where $k_1 = g_c(\mathbf{x} = 0.125)$ and $k_2 = g_{camber}(\mathbf{x} = 0.125)$. An extended review of the two dimensional theory and the mathematical derivation of this method and applications, can be found in Gaunaa (2002, 2006).

$$\frac{\Delta P(0.125)}{q} = k_1\alpha + k_2 \implies \alpha = \frac{1}{k_1}\left(\frac{\Delta P(0.125)}{q} - k_2\right). \tag{4}$$

https://doi.org/10.5194/wes-2020-35
Preprint. Discussion started: 11 February 2020

eawe european academy of wind energy
Open Access WIND ENERGY SCIENCE DISCUSSIONS

Several studies made by Gaunaa (2002); Gaunaa and Andersen (2009); Velte et al. (2012), related the same theory on wing experiments and computational models, with a Risø-B1-18 and NACA64418. Thus, it is assumed that the linearity, applied on the remaining terms, is a good approximation for a Clark Y airfoil shape, which is thinner (11.8%) than the other airfoils where the method was successfully applied.

In order to obtain the constants k_1 and k_2 from Eq. 4, XFOIL calculations were computed. The AoA was swept from $-3°$ to $10°$. The Reynolds number ($2.5\times10^5 \leq Re \leq 3.0\times10^5$) and free transition method ($4 \leq NCrit \leq 12$) influence were studied with no significant changes. Subsequently, a linear curve fit was made between normalized pressure ($\Delta C_P(0.125)$) and the AoA swept. The fit values are $k_1 = 0.23$ and $k_2 = 0.43$.

Finally the AoA was calculated using Eq. 4, where $\Delta P(0.125) = P_{lower}(0.125) - P_{upper}(0.125)$.

Figure 8 shows a good agreement between the pressure distribution from the rotating blade and the computational tool in the estimated angle. The latter agrees with previous works by Ronsten (1992) and Corten (2001), where it was shown that rotation does not have a great impact over the pressure distribution in the attached flow operations points.

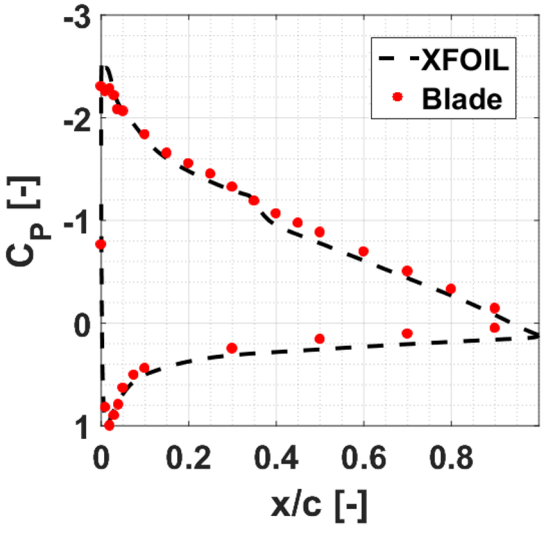

Figure 8. XFOIL ($\alpha = 7.6°$) and measured pressure distribution of the current setup at yaw angle of $\Psi = 0°$, pitch angle of $\theta = 0°$ and azimuth angle of $\phi = 0°$.

Since there are no pressure taps in the exact $12.5\%c$ position, a linear interpolation was made, between $[10-15]\%c$ for the suction side and $[10-30]\%c$ for the pressure side.

The relative dynamic pressure, $q_{rel} = 0.5\rho U_{rel}^2$, was considered equal to the maximum value in pressure side distribution, i.e. at the stagnation point (Shipley et al., 1995), for each azimuth station. This was required for the yaw misalignment cases, where the dynamic pressure is variable with azimuth position.

https://doi.org/10.5194/wes-2020-35
Preprint. Discussion started: 11 February 2020

eawe european academy of wind energy
Open Access WIND ENERGY SCIENCE DISCUSSIONS

3.3.3 Analytic estimation

The introduction of a yaw misalignment produces an expected change in the AoA distribution along the blade span due to the crossflow i.e. depends on the azimuth angle variations. Therefore, a geometrical approach was used to compare the experimental methods under these operational points, as pressure taps and 3-hole probes location differs in radial position.

240 The normal velocity contribution is a function of the yaw angle, Eq. 5. On the contrary, the tangential velocity contribution depends on the rotational speed, yaw and azimuth angle, Eq. 6, due to the crossflow presented (see Fig. 2). Using these geometrical velocities contribution and the axial, a, and tangential, a', factors simulated with the BEM-module QBlade (Marten et al., 2015) an analytical AoA was estimated as is shown in Eq. 7.

$$U_n = U_\infty cos(\psi) \tag{5}$$

245 $$U_t = \Omega r - U_\infty sin(\psi)cos(\phi) \tag{6}$$

$$\alpha_{geo} = atan\left(\frac{U_n(1-a)}{U_t(1+a')}\right) - \theta - \gamma \tag{7}$$

Equation 7 it can be used to estimate the AoA in the aligned case, which is independent of the azimuth angle, as the yaw angle is zero. Therefore the AoA remains constant for the location of the pressure taps and 3-hole probes with a value of $\alpha_{geo,\psi=0^\circ} \approx 5.1^\circ$, when the pitch angle is set at $\theta = 0^\circ$.

https://doi.org/10.5194/wes-2020-35
Preprint. Discussion started: 11 February 2020

eawe european academy of wind energy
Open Access WIND ENERGY SCIENCE DISCUSSIONS

3.4 Test cases and measurement uncertainty

Several operational conditions were analyzed, three yaw angles $\psi = 0°$, $-15°$, and $-30°$, and for each yaw angle, the pitch angle was swept from $-2°$ to $6°$ in steps of $\Delta\theta = 2°$. For all cases, the tip speed ratio was fixed $\lambda = 4.35$.

The uncertainty in the measurement of all quantities was taken into account in order to quantify the magnitude of the errors over the results. The standard deviation was calculated with the same azimuth step as the phase average. The uncertainty due to the filtering (see Fig. 6) was considered as the amplitude of the confidence zone between the filtered, and unfiltered data. The AoA uncertainty is estimated as the error propagation of the phase average and the filter contributions. In the case where the AoA is estimated using the pressure tap measurements (see Eq.4), an additional error propagation step was considered. Table 1 shows the overall uncertainty for all the quantities.

Table 1. Measurement uncertainty summary.

Measurement	FSR	Uncertainty
Yaw angle, Ψ [°]	± 30	$\pm 0.5^a$
Pitch angle, θ [°]	± 15	$\pm 0.5^a$
Azimuth angle, ϕ [°]	$0 - 360$	$\pm 0.5^b$
Dynamic pressure, $[Pa]$	$0 - 60$	$\pm 0.2^c$
Three hole probes:		
Sensortechnics $HCL0075E$ $[Pa]$	± 7500	
Phase standard deviation, [°]	-	$\pm 0.1^c$
Filtering, [°]	-	± 0.2
angle of attack, α [°]	-3 to 12	± 0.2
Pressure taps:		
Sensortechnics $HCL0025E$ $[Pa]$	± 2500	
Phase standard deviation, [°]	-	$\pm 0.2^c$
Filtering, [°]	-	± 0.1
Angle of attack, α [°]	-3 to 12	± 0.3

(a) Minimum permissible. (b) Bin adjacency. (c) Overall average over standard deviation cases.

During the measurement campaign temperature and relative humidity were recorded with values of $18 \pm 1.5°\mathrm{C}$ and $40 \pm 5\%$, respectively. According to Tsilingiris (2008), these values represent small changes in the physical properties, thus, a density correction was neglected.

https://doi.org/10.5194/wes-2020-35
Preprint. Discussion started: 11 February 2020

eawe european academy of wind energy
Open Access WIND ENERGY SCIENCE DISCUSSIONS

4 Results and discussion

The results are presented in this section, starting from the pressure distributions and the relative dynamic pressure along the chord at the span position of $r/R = 0.45$, followed by the comparison between the described methods to determine the AoA. Finally, an additional comparison is presented with the variations of the pitch angle.

4.1 Pressure distribution

The AoA estimation based on the surface pressure measurements depends on the relative dynamic pressure (q_{rel}) and the pressure difference ($\Delta P(12.5\%c)$), see Eq. 4. It is hence important to examine their variation with azimuth position before we proceed to the AoA estimation. Figure 9 shows both the variation of both variables.

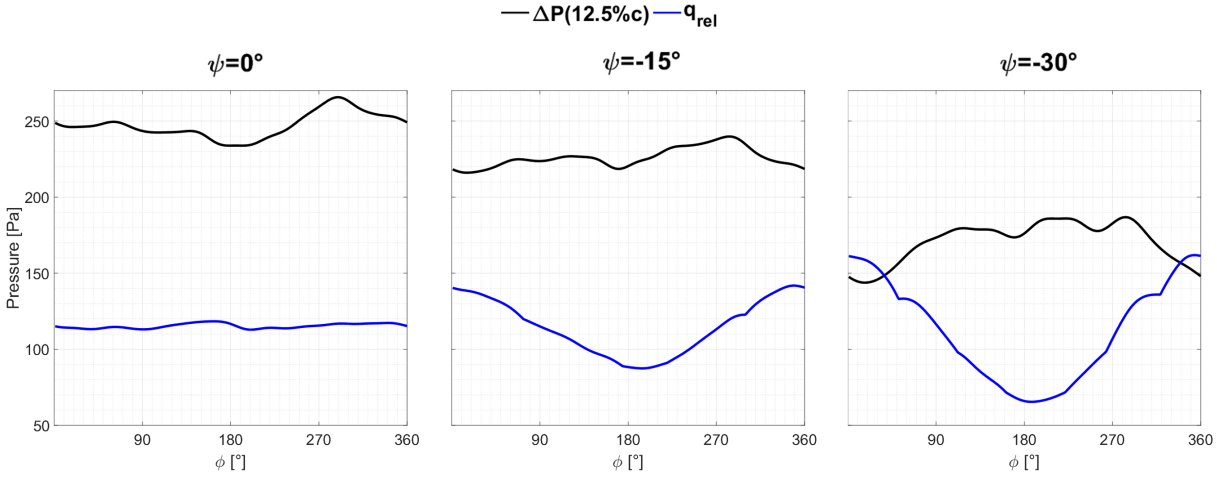

Figure 9. Results from pressure taps at $r/R = 0.45$. For three yaw angles, relative dynamic pressure (q_{rel}) and pressure difference between the pressure and the suction side of the blade at $12.5\%c$ variations with azimuth angle.

For the aligned case, $\psi = 0°$, the relative dynamic pressure remains relatively constant at $q_{rel} \approx 115$Pa with a small increment, $q_{rel} \approx 120$Pa before the azimuth angle $\phi = 180°$ and immediately after a decrement up to $q_{rel} \approx 110$Pa. The latter can be explained by the tower effect, in which the blade is entering to the influence of the tower before the azimuth angle $\phi = 180°$ to afterwards leaving it. The same behavior is observed on the on-blade velocity described by Klein et al. (2018). The pressure difference at $12.5\%c$ remains relatively constant, $\Delta P(12.5\%c) \approx 250$Pa, until the azimuth angle $\phi = 70°$ to after drops continually until the azimuth $\phi = 180°$ where it reaches its minimum, $\Delta P(12.5\%c) = 235$Pa. Thereupon the pressure difference recovers until $\phi = 290°$ reaching its maximum $\Delta P(12.5\%c) = 265$Pa. This behavior agrees qualitatively with computational results made by Schulz et al. (2017), where it is shown an asymmetrical axial load, even without the presence of yaw misalignment.

https://doi.org/10.5194/wes-2020-35
Preprint. Discussion started: 11 February 2020

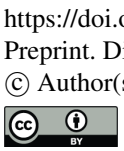

eawe european academy of wind energy
Open Access WIND ENERGY SCIENCE DISCUSSIONS

With the introduction of yaw misalignment $\psi = -15°$, the relative dynamic pressure is influenced by the yaw angle, showing a symmetrical trend with its minimum value at an azimuth angle of $\phi \approx 180°$. The maximum variation is $\Delta q_{rel} = q_{rel,max} - q_{rel,min} \approx 50$ Pa. Regarding the pressure difference at $12.5\%c$ this displays similar features as in the aligned case, but with a shifted azimuth angle position, getting its minimum, $\Delta P(12.5\%c) = 220$ Pa, at $\phi = 170°$ and it maximum, $\Delta P(12.5\%c) = 240$ Pa, at $\phi = 285°$. This behavior suggests being related to the advancing/retreating behavior described by Schulz et al. (2017).

For the case of yaw angle $\psi = -30°$, the relative dynamic pressure behavior remains and the drop increases up to $\Delta q_{rel} \approx 90$ Pa. In the case of the pressure difference at $12.5\%c$ the azimuth angle dependency becomes more important and the advancing/retreating influence is more pronounced.

Regarding the magnitude of the dynamic pressure, q_{rel}, and the location of the stagnation point vary with azimuth position for the misaligned cases. Figure 10 provides an overview of the stagnation point location and the pressure magnitude variation for the different yaw cases in the region close to the leading edge ($0\%c \leq x \leq 4\%c$). The position of the stagnation point at each azimuth angle is indicated on the pressure contours by circles ($\circ$).

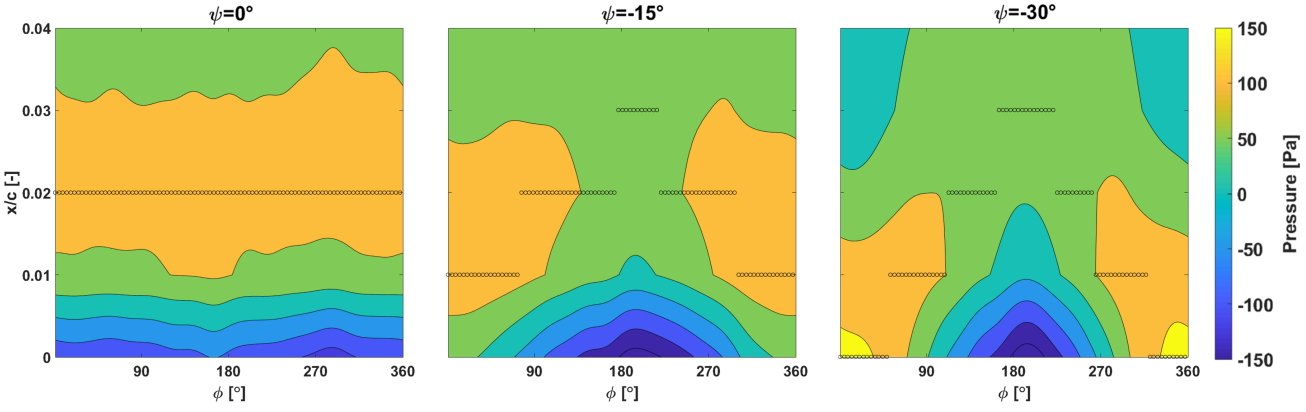

Figure 10. Pressure contours over the pressure side at $r/R = 0.45$ in the range $[0, 4]\%c$ for all yaw cases and pitch angle of $\theta = 0°$. The circles ($\circ$) are located at $max\{P\}$ at that azimuth position and indicate the location of the stagnation point.

It can be seen that for yaw angle $\psi = 0°$ case, Fig. 10 (left), that the relative dynamic pressure position is always at $x = 2\%c$. On the contrary for the yaw angle $\psi = -15°$ case, Fig. 10 (middle), the stagnation point is further upstream ($x = 1\%$) at azimuth angle $\phi = 0°$ and moves downstream towards $x = 3\%$ for $\phi = 180°$, and back to $x = 1\%$ as the blade moves towards the $\phi = 0°$ position. Finally, for the case of yaw $\psi = -30°$, Fig. 10 (right), the behavior of the stagnation point is similar, but more pronounced, between at $x = 0\%$ and $x = 3\%$ at azimuth angles of $\phi = 0°$ and $\phi = 180°$, respectively.

The pressure taps are located at discrete points in the surface this movement in the stagnation point, i.e. in the values of the relative dynamic pressure, this explains the sharp changes present in yaw angle $\psi = -15°$ at azimuth angles $\psi \approx 70°$ and $\phi \approx 300°$ and yaw angle $\psi - 30°$ at azimuth angles of $\phi \approx 50°$ and $\phi \approx 320°$(see Fig. 9).

https://doi.org/10.5194/wes-2020-35
Preprint. Discussion started: 11 February 2020

eawe european academy of wind energy
Open Access WIND ENERGY SCIENCE DISCUSSIONS

Regarding the drop in relative dynamic pressure for the misalignment cases, this can be explained with the geometrical velocities. Equation 8 shows both, normal and tangential contributions, resulting from the relative dynamic pressure $q_{rel,geo} = 0.5\rho U_{rel}^2$ (see Eqs. 5 and 6).

$$\frac{q_{rel,geo}}{0.5\rho U_{\infty}^2} = \underbrace{(cos(\psi))^2}_{normal\ contribution} + \underbrace{(\lambda(r/R) - sin(\psi)cos(\phi))^2}_{tangential\ contribution} \tag{8}$$

Figure 11 shows the relative dynamic pressure at the radial position $r/R = 0.45$ for the misaligned cases ($\psi = -15°$ and $\psi = -30°$) normalized by the aligned case ($\psi = 0°$). It can be seen the same trend between the geometrical case (dashed line) and the estimation from the pressure taps (solid line) as well in the maximum ($\phi = 0°$) and minimum ($\phi = 180°$) azimuth positions.

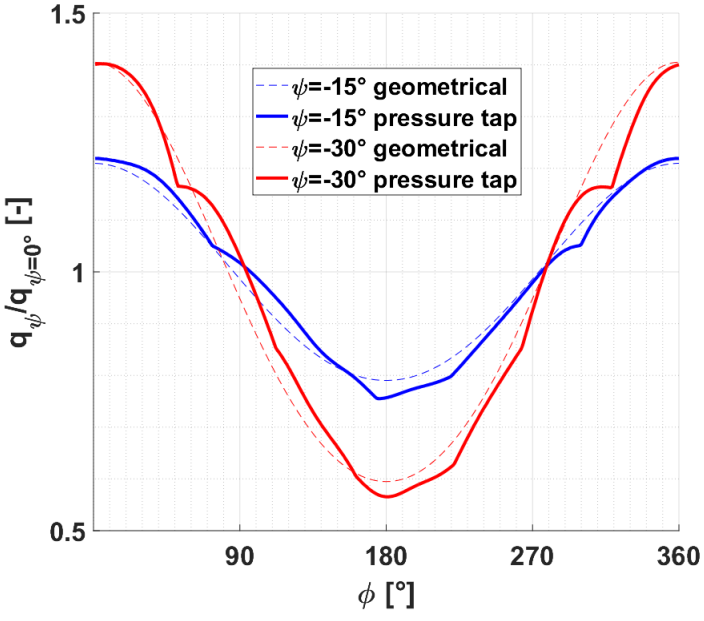

Figure 11. Normalized relative dynamic pressure at radial position $r/R = 0.45$ and yaw misalignment cases of $\psi = -15°$ and $\psi = -30°$. Solid line, pressure tap estimation. Dashed line, geometrical calculation.

https://doi.org/10.5194/wes-2020-35
Preprint. Discussion started: 11 February 2020

eawe european academy of wind energy
Open Access WIND ENERGY SCIENCE DISCUSSIONS

4.2 Angle of attack estimation

4.2.1 Test cases

Figures 12, 13 and 14 show the AoAs results from the pressure tap ($PP\ 45\%R$) and the 3-hole probe ($3HP$) methods over the three yaw angles cases. In the interest of clarity, only one of the pitch angles is presented here for each yaw angle case. For completeness, the results for the remaining pitch cases can be found in App. C and an analysis through the pitch cases is presented in Sect. 4.2.2.

Figure 12 shows the AoA for the pitch angle $\theta = 0°$ in the aligned case. It can be seen that the two approaches are able to capture the tower influence, which produces a reduction of the AoA around the azimuth angle of $\phi = 180°$. However, the AoA from the 3-hole probes method capture a drop near the zone of azimuth angle $\phi \approx 100°$ and several more with different intensities along with azimuth angle variations. This behavior has been seen in previous results of Klein et al. (2018); Bartholomay et al. (2018b); Marten et al. (2018) and is related to small mounting errors and vibrations of the probes.

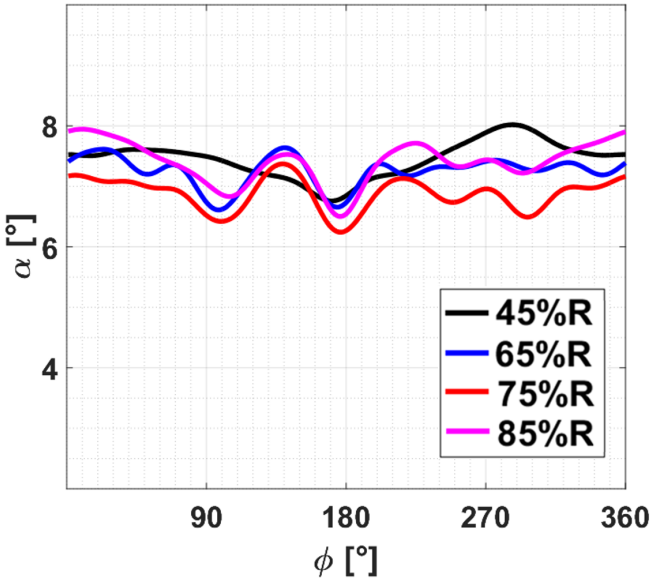

Figure 12. AoA results from pressure taps and 3-hole probe approaches. Yaw angle $\psi = 0°$ and pitch angle $\theta = 0°$.

Although the AoA over the azimuthal variation is not constant, both methods estimate a similar AoA range. The AoA for both pressure tap and 3-hole probe methods are slightly lower than previous results show by Klein et al. (2018), but within the uncertainty values. As is shown in the mentioned work, the AoA remains relatively constant along the midspan of the blade ($0.5 \leq r/R \leq 0.8$) and larger outside this range which is the case that shows Table 2 for the pressure taps and the 3-hole probe located at 45%R and 85%R, respectively. However, the average AoA, $\overline{\alpha}_{PP}$, has an offset of $\Delta\alpha_{off} = 2.3°$ respect to the analytical AoA $\alpha_{geo,\psi=0°} \approx 5.1$. This overprediction is the result of the wind tunnel walls, which are not included in the

https://doi.org/10.5194/wes-2020-35
Preprint. Discussion started: 11 February 2020

eawe european academy of wind energy
Open Access WIND ENERGY SCIENCE DISCUSSIONS

QBlade simulations, therefore a high blockage in the wind tunnel ($\approx 40\%$) leads to a higher velocity around the rotor, which increases the AoA (Marten et al., 2018).

Additionally, Table 2 shows a comparison between the pressure tap and each 3-hole probe. The overall average AoA difference, $\overline{\Delta\alpha} = mean\{|\alpha_{PP} - \alpha_{3HP}|\}$, for all pitch cases shows that there is a small difference between the pressure tap and 3-hole probe methods, up to $\overline{\Delta\alpha} = 0.8°$. Whereas the AoA maximum difference, $\Delta\alpha_{max} = max\{|\alpha_{PP} - \alpha_{3HP}|\}$, located around the azimuth angles of $\phi = 90°$, and $\phi = 270°$, can take values up to $\Delta\alpha_{max} = 1.7°$. However, this difference is in the same magnitude that the AoA range between minimum and maximum that presents each measurement individually.

Table 2. AoA from the pressure taps and 3-hole probe methods at yaw angle $\psi = 0°$. Average, minimum and maximum for the pitch angle case $\theta = 0°$ and overall comparison for all pitch cases.

Method	$\overline{\alpha}$ [°]	α_{min} [°]	α_{max} [°]	PP comparison		
PP 45%R	7.4	6.8	8.0	$\Delta\alpha_{max}$ [°]	$\overline{\Delta\alpha}$ [°]	$std(\Delta\alpha)$ [°]
$3HP$ 65%R	7.3	6.6	7.6	1.2	0.4	0.2
$3HP$ 75%R	6.9	6.2	7.4	1.7	0.8	0.3
$3HP$ 85%R	7.4	6.5	7.9	1.3	0.4	0.2

Figure 13 shows the AoA from the pressure tap and 3-hole probe methods (left), and analytical calculations (right) for the pitch angle $\theta = 0°$ and the yaw misalignment of $\psi = -15°$.

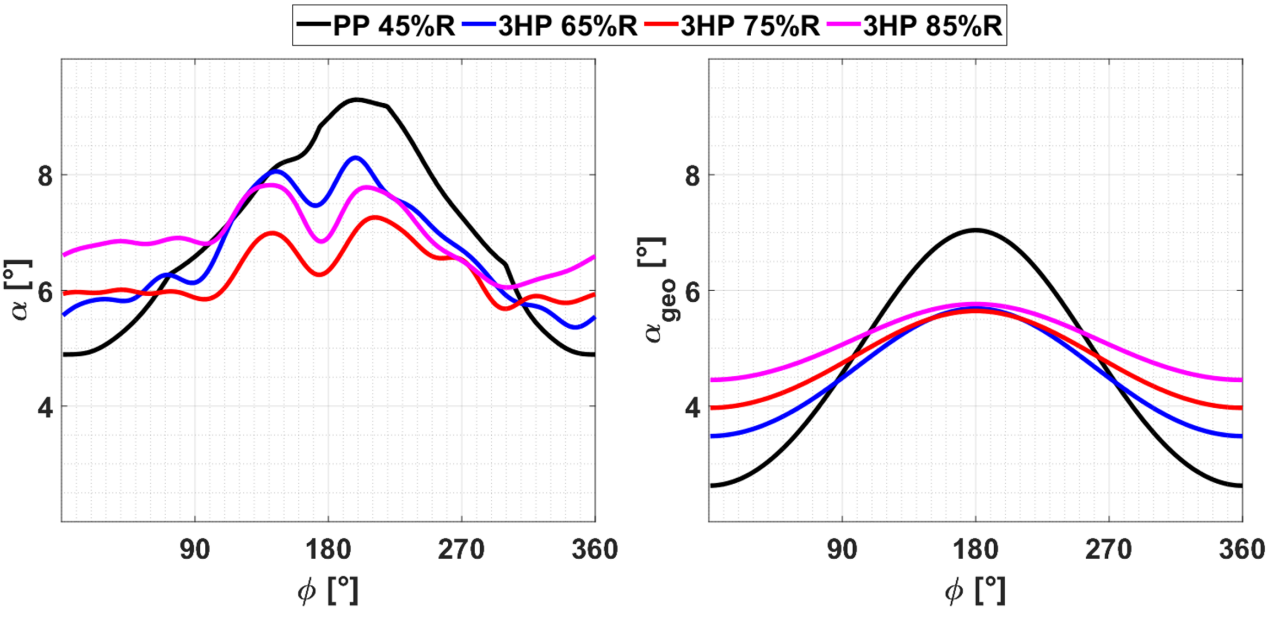

Figure 13. AoA results for yaw angle $\psi = -15°$ and pitch angle $\theta = 0°$. Pressure taps and 3-hole probe approaches (left). Analytical calculations (right).

https://doi.org/10.5194/wes-2020-35
Preprint. Discussion started: 11 February 2020

eawe european academy of wind energy
Open Access WIND ENERGY SCIENCE DISCUSSIONS

From Fig. 13 (left) it can be noticed that the AoA estimation from the pressure tap starts with smaller values until azimuth angle $\phi \approx 70°$ where becomes larger than the AoA from the 3-hole probes estimation. The 3-hole probe approach still shows the tower influence with a drop in the AoA around the azimuth angle $\phi = 180°$, in contrast with the pressure tap method, where the AoA keeps increasing until the maximum position located in azimuth angle of $\phi \approx 200°$, except for a small perturbance at azimuth angle $\phi = 170°$. A reduction in the AoA is followed where the pressure tap estimation becomes smaller than the 3-hole probe approach, as the blade is moving towards the azimuth angle $\phi = 0°$.

The same behavior is presented in the case of analytical AoA, Fig. 13 (right) with two main differences, first, there is no tower effect, due to the analytical approach does not take this consideration and second, an offset AoA between the curves is appreciated, as the aligned case, with a value of $\alpha_{off} \approx 2.3°$, which is still explained by the blockage effect due that the misalignment only reduces the level of blockage from 40% to $\approx 39\%$.

For this yaw misalignment, it is shown that the 3-hole probe has a trend less pronounced than the pressure tap approach between $0° \leq \phi \leq 90°$ and $270° \leq \phi \leq 360°$. Furthermore, the crossflow has covered partially the influence of the tower in the pressure tap method, increasing the AoA disagreement between both methods is in the azimuth angle range $135° \leq \phi \leq 225°$.

Figure 14 shows the AoA from the pressure tap and 3-hole probe methods (left), and analytical calculations (right) for the pitch angle $\theta = 0°$ and the yaw misalignment of $\psi = -30°$.

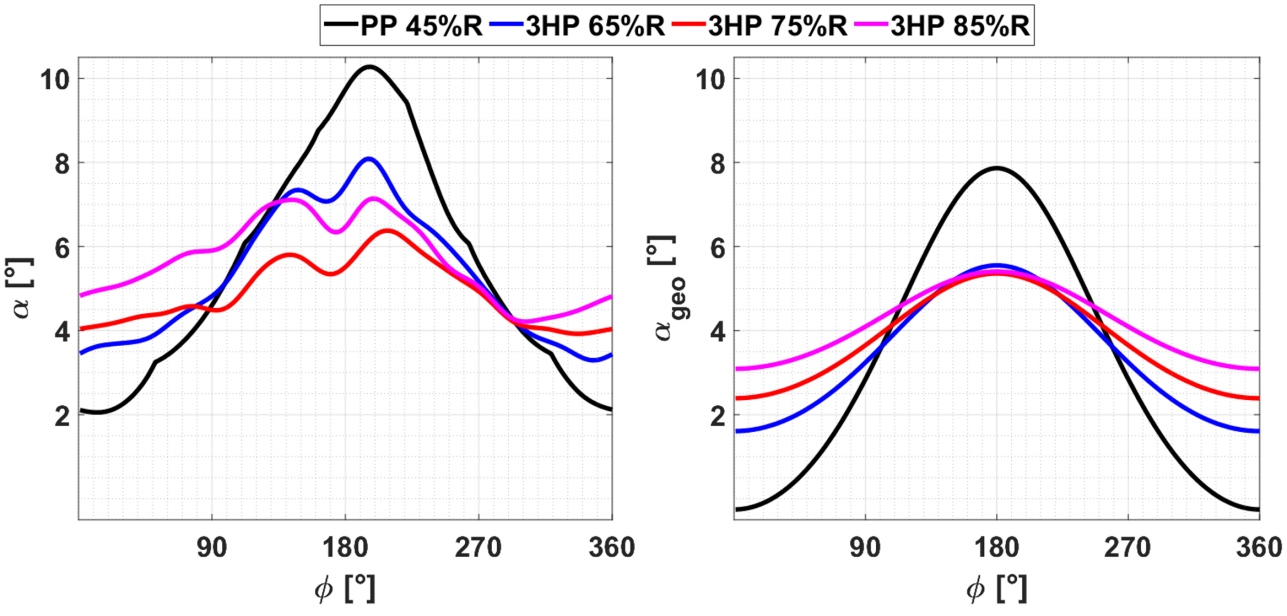

Figure 14. AoA results for yaw angle $\psi = -30°$ and pitch angle $\theta = 0°$. Pressure taps and 3-hole probe approaches (left). Analytical calculations (right).

The behavior of the AoA results from the pressure tap method, Fig. 14 (left), in this case, is similar to the yaw angle $\psi = -15°$, exhibiting a more pronounced difference with the 3-hole probe approach in the azimuth angle $\phi = 180°$. The effect

https://doi.org/10.5194/wes-2020-35
Preprint. Discussion started: 11 February 2020

eawe european academy of wind energy
Open Access WIND ENERGY SCIENCE DISCUSSIONS

of the crossflow due to the yaw misalignment is dominant in this case, diminishing the AoA drop around the azimuth angle $\phi = 180°$ in the 3-hole probe and vanishing it in the case of the pressure tap, in contrast with the previous yaw case.

Regarding the analytical AoA, Fig. 14 (right), the AoA show the same features, including the larger difference in AoA for the azimuth angles $\phi = 0°$ and $\phi = 180°$. Moreover, the offset between both results remains. This offset was previously showed for different QBlade results by Klein et al. (2018); Marten et al. (2018) under aligned and misaligned conditions, where the AoA from QBlade estimations was always smaller than when the wind tunnel walls were included.

4.2.2 Pitch analysis

A comparison between the AoA estimations from both approaches trough the pitch angle cases, in a fixed azimuth position, $\phi = 315°$, was analyzed. Figure 15 shows the evolution of AoA estimations at the azimuth angle of $\phi = 315°$. It can be observed that the trend is linear for both methods. While the yaw angle increases the pressure tap method change from estimate larger to smaller values than 3-hole probes.

A linear fit $\alpha = m\theta + k$ was obtained, in order to check the relation between AoA and pitch angle. The slopes take values around $m = -0.7 \pm 0.1[1/°]$. From the geometrical point of view (see Eq. 7), the expected slope between the AoA and pitch is $m = -1$. Nevertheless, both measurement tools capture the influence of the pitch change into the induction factors, which also explain the change in the slope between methods (i.e. radial positions) and yaw misalignments, where should be expected a non-uniform induction factor along the blade (Schepers, 2012).

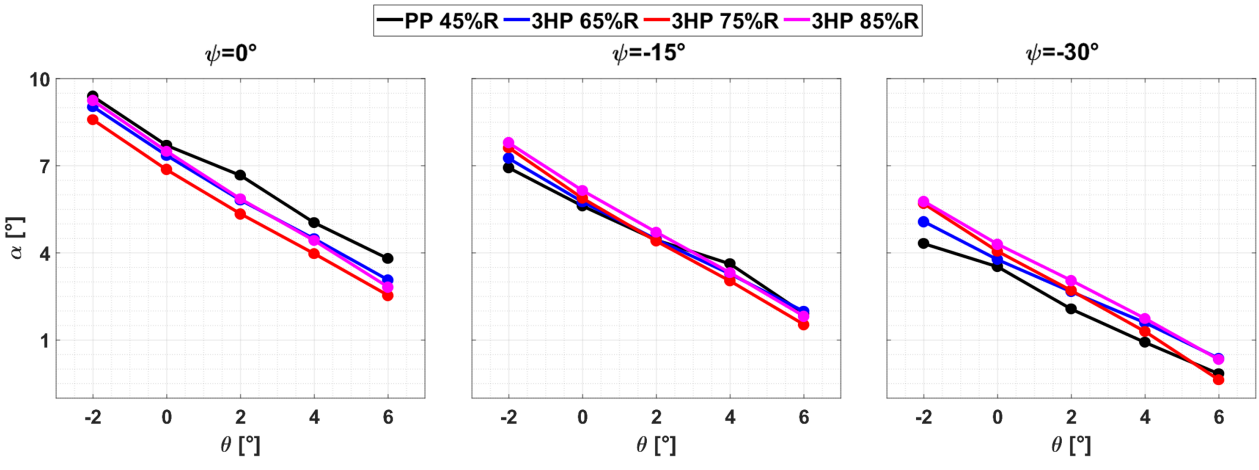

Figure 15. AoA estimations from pressure tap and 3-hole probe methods, variations with pitch angle. Three yaw cases $\psi = 0, -15, -30°$.

https://doi.org/10.5194/wes-2020-35
Preprint. Discussion started: 11 February 2020

eawe european academy of wind energy
Open Access WIND ENERGY SCIENCE DISCUSSIONS

5 Conclusions

A method to determine the AoA based on the pressure difference between the pressure and suction side on a wind turbine blade was tested. The method was compared with the AoA results from three 3-hole probes in simultaneous wind tunnel measurements together with analytical calculations. Several conditions were studied regarding the introduction of yaw misalignment and different pitch angles for the blades.

The pressure distribution on the blade at $45\%R$ was measured trough chordwise pressure taps. The tested method uses the information of a reduced number of pressure taps located close to the blade leading edge in order to estimate the relative dynamic pressure to its corresponding blade section. Additionally, the pressure difference between suction and pressure side of the blade at $12.5\%c$ is tracked in order to determine the AoA based on 2-D assumptions.

The results show that in the aligned case, $\psi = 0°$, the pressure tap approach is suitable, being capable of capturing the same features of the AoA results from the 3-hole probes, including the influence of the tower effect. The comparison between the pressure tap method and the three 3-hole probes present a maximum overall average difference of $\overline{\Delta\alpha} = 0.8$. Moreover, the AoA results from the pressure tap method present a smoother and stable trend than the results from the 3-hole probe approach, which can be produced by a consequence of vibrations of the latter.

With the introduction of yaw misalignment, the AoA results from the pressure tap method show, as expected, the crossflow influence in a more pronounced curve than the 3-hole probe, in agreement with the analytical results. The crossflow impact is more dominant than the tower effects and the pressure tap method is not able to predict its influence, from where it can be inferred an AoA overestimation in the azimuth region of $135° \leq \phi \leq 225°$.

Regarding the pitch angle changes in the blades, the AoA results from the pressure tap approach presents a linear behavior with a slope value of $m = 0.7 \pm 0.1[1/°]$, similarly to the 3-hole probe method, being capable to capture the resulting effects from the axial and tangential induction.

Overall, it is found that the pressure tap method applied here to determine the AoA, provides reliable data, with good performance for both aligned and misaligned cases. This is a significant step that eliminates the need for external probes, which affect the flow over the blade and require additional calibration.

Data availability. Pressure measurement data and results can be provided by contacting the corresponding author

https://doi.org/10.5194/wes-2020-35
Preprint. Discussion started: 11 February 2020

References

Bak, C., Troldborg, N., and Madsen, H. A.: DAN-AERO MW: Measured airfoil characteristics for a MW rotor in atmospheric conditions, in: EWEA Annual Event 2011, European Wind Energy Association (EWEA), 2011.

Bartholomay, S., Fruck, W.-L., Pechlivanoglou, G., Nayeri, C. N., and Paschereit, C. O.: Reproducible Inflow Modifications for a Wind Tunnel Mounted Research Hawt, in: ASME Turbo Expo 2017: Turbomachinery Technical Conference and Exposition, pp. V009T49A013–V009T49A013, American Society of Mechanical Engineers, 2017.

Bartholomay, S., Marten, D., Martínez, M. S., Alber, J., Pechlivanoglou, G., Nayeri, C. N., Paschereit, C. O., Klein, A. C., Lutz, T., and Krämer, E.: Cross-Talk Compensation for Blade Root Flap-and Edgewise Moments on an Experimental Research Wind Turbine and Comparison to Numerical Results, in: ASME Turbo Expo 2018: Turbomachinery Technical Conference and Exposition, pp. V009T48A016–V009T48A016, American Society of Mechanical Engineers, 2018a.

Bartholomay, S., Michos, G., Perez-Becker, S., Pechlivanoglou, G., Nayeri, C., Nikolaouk, G., and Paschereit, C. O.: Towards Active Flow Control on a Research Scale Wind Turbine Using PID controlled Trailing Edge Flaps, in: 2018 Wind Energy Symposium, p. 1245, 2018b.

Bechmann, A., Sørensen, N. N., and Zahle, F.: CFD simulations of the MEXICO rotor, Wind Energy, 14, 677–689, 2011.

Bergh, H. and Tijdeman, H.: Theoretical and experimental results for the dynamic response of pressure measuring systems, Tech. rep., Nationaal lucht-en ruimtevaartlaboratorium, 1965.

Corten, G. P.: Flow separation on wind turbines blades, Ph.D. thesis, Universiteit Utrecht, Nederland, 2001.

Drela, M. and Youngren, H.: XFOIL; Subsonic Airfoil Development System, https://web.mit.edu/drela/Public/web/xfoil/, 2001.

Dudzinski, T. J. and Krause, L. N.: Flow-direction measurement with fixed-position probes, Tech. rep., NASA TM X-1904, 1969.

Gallant, T. and Johnson, D.: In-blade angle of attack measurement and comparison with models, in: Journal of Physics: Conference Series, vol. 753, p. 072007, IOP Publishing, 2016.

Gaunaa, M.: Unsteady aerodynamic forces on NACA 0015 airfoil in harmonic translatory motion, Technical University of Denmark,(MEK-FM-PHD, 2002.

Gaunaa, M.: Unsteady 2D potential-flow forces on a thin variable geometryairfoil undergoing arbitrary motion., Tech. rep., Risø-R-1478(EN), 2006.

Gaunaa, M. and Andersen, P. B.: Load reduction using pressure difference on airfoil for control of trailing edge flaps, in: 2009 European Wind Energy Conference and Exhibition, EWEC, 2009.

Guntur, S. and Sørensen, N. N.: An evaluation of several methods of determining the local angle of attack on wind turbine blades, in: The science of Making Torque from Wind 2012: 4th scientific conference, 2012.

Hand, M., Simms, D., Fingersh, L., Jager, D., Cotrell, J., Schreck, S., and Larwood, S.: Unsteady aerodynamics experiment phase VI: wind tunnel test configurations and available data campaigns, Tech. rep., National Renewable Energy Lab., Golden, CO.(US), 2001.

Klein, A. C., Bartholomay, S., Marten, D., Lutz, T., Pechlivanoglou, G., Nayeri, C. N., Paschereit, C. O., and Krämer, E.: About the suitability of different numerical methods to reproduce model wind turbine measurements in a wind tunnel with a high blockage ratio, Wind Energy Science, 3, 349–460, 2018.

Larsen, T. J. and Hansen, A. M.: How 2 HAWC2, the user's manual, Tech. rep., Roskilde, Denmark:, 2007.

Maeda, T. and Kawabuchi, H.: Surface pressure measurement on a rotating blade of field horizontal axis wind turbine in yawed condition, JSME International Journal Series B Fluids and Thermal Engineering, 48, 156–163, 2005.

https://doi.org/10.5194/wes-2020-35
Preprint. Discussion started: 11 February 2020

Maeda, T., Ismaili, E., Kawabuchi, H., and Kamada, Y.: Surface pressure distribution on a blade of a 10 m diameter hawt (field measurements versus wind tunnel measurements), Journal of solar energy engineering, 127, 185–191, 2005.

Maeda, T., Kamada, Y., Suzuki, J., and Fujioka, H.: Rotor blade sectional performance under yawed inflow conditions, Journal of Solar Energy Engineering, 130, 031 018, 2008.

Marten, D., Lennie, M., Pechlivanoglou, G., Nayeri, C. N., and Paschereit, C. O.: Implementation, optimization and validation of a nonlinear lifting line free vortex wake module within the wind turbine simulation code QBlade, in: ASME Turbo Expo 2015: Turbine Technical Conference and Exposition, American Society of Mechanical Engineers Digital Collection, 2015.

Marten, D., Bartholomay, S., Pechlivanoglou, G., Nayeri, C., Paschereit, C. O., Fischer, A., and Lutz, T.: Numerical and Experimental Investigation of Trailing Edge Flap Performance on a Model Wind Turbine, in: 2018 Wind Energy Symposium, p. 1246, 2018.

Marten, D., Paschereit, C. O., Huang, X., Meinke, M. H., Schroeder, W., Mueller, J., and Oberleithner, K.: Predicting Wind Turbine Wake Breakdown Using a Free Vortex Wake Code, in: AIAA Scitech 2019 Forum, p. 2080, 2019.

Morote, J.: Angle of attack distribution on wind turbines in yawed flow, Wind Energy, 19, 681–702, 2016.

Pechlivanoglou, G., Fischer, J., Eisele, O., Vey, S., Nayeri, C., and Paschereit, C.: Development of a medium scale research hawt for inflow and aerodynamic research in the tu berlin wind tunnel, in: 12th German Wind Energy Conference (DEWEK), Bremen, Germany, May, pp. 19–20, 2015.

Petersen, M., Larsen, T., Madsen, H., Larsen, G., and Toldborg, N.: Turbulent wind field characterization and re-generation based on pitot tube measurements mounted on a wind turbine, Tech. rep., Department of Wind Energy, Technical University of Denmark, 2015.

Ronsten, G.: Static pressure measurements on a rotating and a non-rotating 2.375 m wind turbine blade. Comparison with 2D calculations, Journal of Wind Engineering and Industrial Aerodynamics, 39, 105–118, 1992.

Sant, T., van Kuik, G., and Van Bussel, G.: Estimating the angle of attack from blade pressure measurements on the NREL phase VI rotor using a free wake vortex model: axial conditions, Wind Energy: An International Journal for Progress and Applications in Wind Power Conversion Technology, 9, 549–577, 2006a.

Sant, T., van Kuik, G., and van Bussel, G.: Estimating the Unsteady Angle of Attack from Blade Pressure Measurments on the NREL Phase VI Rotor in Yaw using a Free-Wake Vortex Model, in: 44th AIAA Aerospace Sciences Meeting and Exhibit, p. 393, 2006b.

Sant, T., van Kuik, G., and Van Bussel, G.: Estimating the angle of attack from blade pressure measurements on the National Renewable Energy Laboratory phase VI rotor using a free wake vortex model: yawed conditions, Wind Energy: An International Journal for Progress and Applications in Wind Power Conversion Technology, 12, 1–32, 2009.

Schepers, J. G.: Engineering models in wind energy aerodynamics: Development, implementation and analysis using dedicated aerodynamic measurements, Ph.D. thesis, Delft University of Technology, 2012.

Schmid, M.: A fiber-optic sensor for measuring quasi-static and unsteady pressure on wind energy converters, in: 4SMARTS-Symposium für Smarte Strukturen und Systeme, Braunschweig, 22.06. 2017, 2017.

Schulz, C., Letzgus, P., Lutz, T., and Krämer, E.: CFD study on the impact of yawed inflow on loads, power and near wake of a generic wind turbine, Wind Energy, 20, 253–268, 2017.

Shen, W. Z., Hansen, M. O., and Sørensen, J. N.: Determination of the angle of attack on rotor blades, Wind Energy: An International Journal for Progress and Applications in Wind Power Conversion Technology, 12, 91–98, 2009.

Shipley, D. E., Miller, M. S., Robinson, M. C., Luttges, M. W., and Simms, D. A.: Techniques for the determination of local dynamic pressure and angle of attack on a horizontal axis wind turbine, Tech. rep., National Renewable Energy Lab., Golden, CO (United States), 1995.

https://doi.org/10.5194/wes-2020-35
Preprint. Discussion started: 11 February 2020

Sicot, C., Devinant, P., Loyer, S., and Hureau, J.: Rotational and turbulence effects on a wind turbine blade. Investigation of the stall mechanisms, Journal of wind engineering and industrial aerodynamics, 96, 1320–1331, 2008.

Tsilingiris, P.: Thermophysical and transport properties of humid air at temperature range between 0 and 100 C, Energy Conversion and Management, 49, 1098–1110, 2008.

Velte, C. M., Mikkelsen, R. F., Sørensen, J. N., Kaloyanov, T., and Gaunaa, M.: Closed loop control of a flap exposed to harmonic aerodynamic actuation, in: The science of Making Torque from Wind 2012: 4th scientific conference, 2012.

Vey, S., Marten, D., Pechlivanoglou, G., Nayeri, C., and Paschereit, C. O.: Experimental and numerical investigations of a small research wind turbine, in: 33rd AIAA Applied Aerodynamics Conference, p. 3392, 2015.

https://doi.org/10.5194/wes-2020-35
Preprint. Discussion started: 11 February 2020

eawe european academy of wind energy
Open Access WIND ENERGY SCIENCE DISCUSSIONS

Appendix A: List of symbols

AoA, α	Angle of attack
U	Velocity
ψ	Yaw angle
ϕ	Azimuth angle
λ	Tip speed ratio
f	Rated frequency
R	Rotor radius
$BeRT$	Berlin Research Turbine
γ	Twist angle
θ	Pitch angle
c	Chord length
r/R	Nondimensional radial blade position [0,1]
x	Horizontal chord position
$\mathbf{x}$	Nondimensional chordwise coordinate [0,1]
y	Vertical chord position
X	Axial wind tunnel position
Y	Lateral wind tunnel position
R^2	Coefficient of determination
ρ	Air density
Ω	Angular velocity
q	Dynamic pressure
g	Gaunaa model contribution in pressure distribution
β	Flap angle
k	Fit constant
PP	Pressure taps method
$3HP$	3-hole probe method
FSR	Full Scale Range

https://doi.org/10.5194/wes-2020-35
Preprint. Discussion started: 11 February 2020

eawe european academy of wind energy
Open Access WIND ENERGY SCIENCE DISCUSSIONS

Appendix B: Subscripts

∞	Free stream
ref	Reference value
$upper$	Blade section suction side
$lower$	Blade section pressure side
s	sensor
$corr$	Corrected value
ctf	Centrifugal
$probe$	In reference of probe coordinate system
$probe, section$	In reference of blade section coordinate system
rel	Relative
c	Circulatory
eff	Effective
$camb$	Camber
L	Nonlinear terms
off	Offset
t	Tangential
n	Normal

https://doi.org/10.5194/wes-2020-35
Preprint. Discussion started: 11 February 2020

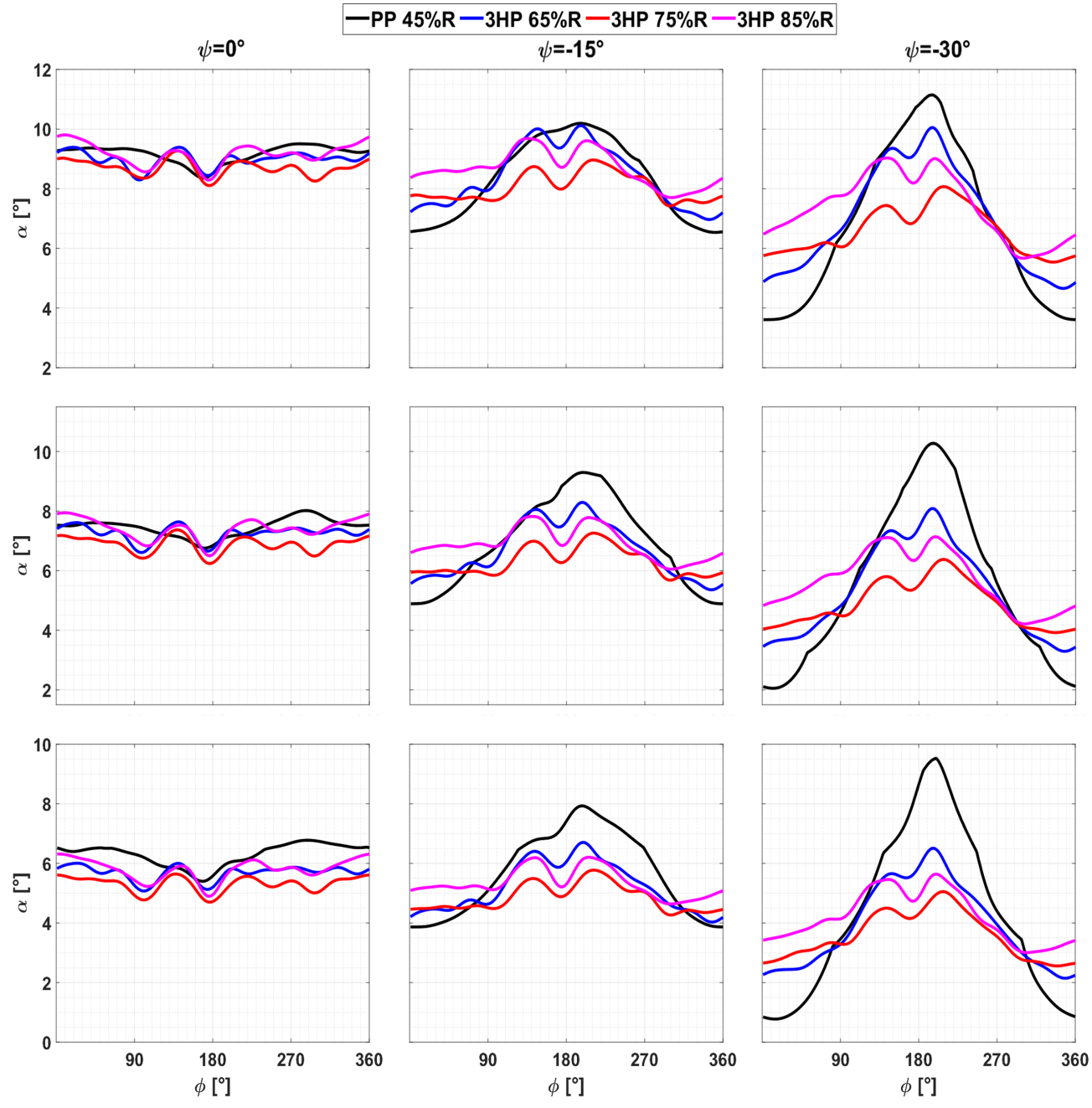

Figure C1. AoA results from the pressure tap and 3-hole probe approaches. In columns yaw angles: $\psi = 0°$, $\psi = -15°$ and $\psi = -30°$. In rows pitch angles: $\theta = -2°$, $\theta = 0°$ and $\theta = 2°$.

Appendix C: Angles of attack

https://doi.org/10.5194/wes-2020-35
Preprint. Discussion started: 11 February 2020

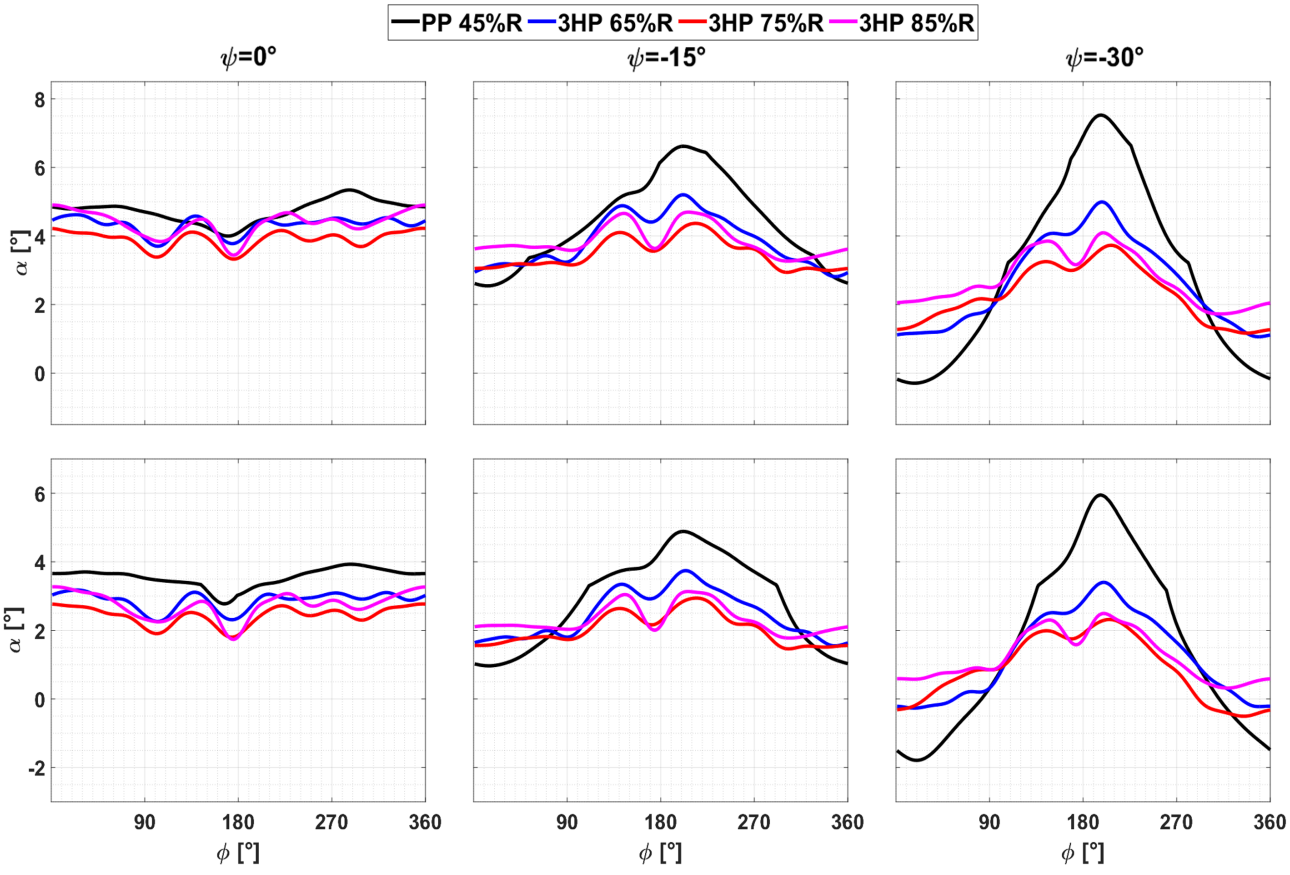

Figure C2. AoA results from the pressure tap and 3-hole probe approaches. In columns yaw angles: $\psi = 0°$, $\psi = -15°$ and $\psi = -30°$. In rows pitch angles: $\theta = 4°$ and $\theta = 6°$.

Author contributions. RSV carried out the measurement campaign with the support of JA and SB. RSV worked in the implementation of the pressure tap method, performed the calculations, analysis and wrote the paper. SB provided the code for the 3 -hole probe method. JA, SB, MM, CNN, and COP contributed with comments and discussions about each section in the manuscript.

Competing interests. The authors declare that they have no conflict of interest.

Acknowledgements. The author would like to thank the support of CONICYT PFCHA/Becas Chile-DAAD/2017 − 91645539. The researchers would also like to acknowledge Joseph Saverin for providing interesting feedback.